AGU PUBLICATIONS

Geochemistry, Geophysics, Geosystems

RESEARCH ARTICLE
10.1002/2016GC006455

Time scales of foam stability in shallow conduits: Insights from analogue experiments

L. Spina[1], B. Scheu[1], C. Cimarelli[1], A. Arciniega-Ceballos[2], and D.B. Dingwell[1]

[1]Department für Geo- und Umweltwissenschaften, Ludwig-Maximilians-Universität München, Munich, Germany, [2]Department of Volcanology, Institute of Geophysics, Universidad Nacional Autónoma de México, Mexico City, Mexico

Key Points:
- The time scale of foam outgassing decreases with increasing particle content and decreasing liquid viscosity
- Dynamic conditions (i.e., bubble growth and strain rate) significantly affect outgassing time scales
- Analogous observations in the degassing style of magma/lava indicate a possible source mechanism for gas-piston events

Supporting Information:
- Supporting Information S1
- Movie S1
- Movie S2
- Movie S3

Correspondence to:
L. Spina,
laura.spina@min.uni-muenchen.de

Citation:
Spina, L., B. Scheu, C. Cimarelli, A. Arciniega-Ceballos, and D.B. Dingwell (2016), Time scales of foam stability in shallow conduits: Insights from analogue experiments, *Geochem. Geophys. Geosyst.*, *17*, 4179–4194, doi:10.1002/2016GC006455.

Received 25 MAY 2016
Accepted 30 SEP 2016
Accepted article online 4 OCT 2016
Published online 27 OCT 2016

Abstract Volcanic systems can exhibit periodical trends in degassing activity, characterized by a wide range of time scales. Understanding the dynamics that control such periodic behavior can provide a picture of the processes occurring in the feeding system. Toward this end, we analyzed the periodicity of outgassing in a series of decompression experiments performed on analogue material (argon-saturated silicone oil plus glass beads/fibers) scaled to serve as models of basaltic magma. To define the effects of liquid viscosity and crystal content on the time scale of outgassing, we investigated both: (1) pure liquid systems, at differing viscosities (100 and 1000 Pa s), and (2) particle-bearing suspensions (diluted and semidiluted). The results indicate that under dynamic conditions (e.g., decompressive bubble growth and fluid ascent within the conduit), the periodicity of foam disruption may be up to several orders of magnitude less than estimates based on the analysis of static conditions. This difference in foam disruption time scale is inferred to result from the contribution of bubble shear and bubble growth to inter-bubble film thinning. The presence of particles in the semidiluted regime is further linked to shorter bubble bursting times, likely resulting from contributions of the presence of a solid network and coalescence processes to the relative increase in bubble breakup rates. Finally, it is argued that these experiments represent a good analogue of gas-piston activity (i.e., the periodical rise-and-fall of a basaltic lava lake surface), implying a dominant role for shallow foam accumulation as a source process for these phenomena.

1. Introduction

Volcanic activity observed at the Earth's surface is a complex result of a wide range of phenomena occurring in the plumbing system. For the common case of the eruption of foamed magmas, the stability of magmatic foam plays a primary role in influencing their eruptive behavior [e.g., *Wilson et al*., 1980]. Indeed, even the origin of explosive basaltic eruptions has generally been related to the ascent of large gas pockets described either via the rise speed model [e.g., *Wilson and Head*, 1981] or the foam collapse model [e.g., *Jaupart and Vergniolle*, 1989]. The former assumes that coalescence occurs during bubble ascent within the conduit, leading to the formation of slugs. The latter, on the contrary, invokes the periodical collapse of a magmatic foam at the roof of the magma chamber to explain the development of slug-bubbles, then rising through the conduit and bursting at the surface. Combined models have been proposed in the literature, under the assumption that irregularities of the geometry of the conduit, such as local inclination or cross-section constriction and horizontal branching, are capable of promoting cascading foam collapses [e.g., *James et al*., 2013]. At the degree of complexity commonly characteristic of natural volcanic systems, geophysical data reveal that more than one process can be active at the same time [e.g., *Bani et al*., 2013; *Spina et al*., 2016a] and the instability of magmatic foam might be a source of some geophysical signals. The periodical collapse of a foam layer in the magma column at Galeras volcano, for example, was identified as source of long-period (LP) events based on correlation analysis between the average LP lapse time and the theoretically expected foam collapse time [*Cruz and Chouet*, 1997].

Despite the substantial literature dealing with magmatic foams and their collapse time scales [e.g., *Jaupart and Vergniolle*, 1989; *Proussevitch et al*., 1993], several questions remain yet unanswered. In particular, the importance of understanding how dynamic conditions (i.e., decompressive bubble growth and fluid ascent within the conduit) affect the final time scale of collapse is apparent. It follows from the above that an

Table 1. List of the Performed Experiments[a]

Exp. Name	Fluid Viscosity (Pa s)	Particle Content (vol %)	Particle Shape	Bubble Radii (mm)[b]	Volume Gas/Total Sample Volume (±0.01)[c]
#3	100	0		0.7–3.8	0.26
#4	100	0		0.05–3.2	0.20
#5	1000	0		0.4–3.1	0.29
#8	100	1	Spherical	0.5–1.7	0.51
#9	100	10	Spherical	0.33–1.1	0.48
#10	100	20	Spherical	Not detectable	0.47
#14	100	0.3	Elongated	0.3–1.5	0.37
#15	100	3	Elongated	0.2–2.4	0.49
#16	100	7	Elongated	Not detectable	0.45
#26	1000	0		0.2–3.2	0.41
#27	1000	0		0.6–3.6	0.41

[a]#3 to #16 are taken from *Spina et al.* [2016]. The samples were saturated with Argon gas for 72 h at 10 MPa (9.5 MPa for experiment #3).
[b]Range of bubble radii measured at the base of the foam at different time during the foam oscillation phase. Note that the range is not exhaustive over the whole bubble population.
[c]Calculated as incremental volume from the initial full liquid sample. The maximum error originates from the assumption of a flat interface in the volume computation.

accurate description of system properties (i.e., presence of particles and fluid viscosity) and the temporal evolution of the foam will be required to better constrain the source processes of cyclic activity frequently observed at active volcanoes.

Periodicity in eruptive activity, with different time scales spanning from minutes to hours up to years, has been widely reported for subaerial (e.g., Soufriere Hills Volcano [*Druitt et al.*, 2002]), submarine (e.g., Monowai Volcano [*Chadwick et al.*, 2008]), and even extraterrestrial volcanoes (e.g., Loki [*Rathbun et al.*, 2002]). Among the different styles of cyclic degassing at basaltic systems, a well-known case is the so-called gas-piston activity, typically expressed in the cyclic rise-and-fall of a lava lake surface [i.e., *Swanson et al.*, 1979]. Despite abundant literature dealing with the modeling of gas pistons [*Orr and Rea*, 2012, and references therein], the mechanism governing the cyclical uprising of the lava column is still debated. Geologic observations and geophysical data have yielded inconsistent models [*Marchetti and Harris*, 2008]. The introduction of laboratory experiments into this debate offers the hope of further elucidating the source processes of such cyclic degassing phenomena at basaltic volcanoes.

Here we have investigated in detail the periodicity in the outgassing of analogue magmatic foams generated during decompression experiments. The general degassing response of the mixtures to decompression and their rheological properties have been analyzed in a companion paper by *Spina et al.* [2016b]. In the present paper, we address the final stage of the foam evolution, characterized by cyclic degassing style. In particular, we focus on a subset of analogue samples, with different physical properties (i.e., liquid viscosity and particle content) to investigate the effect of dynamic and material parameters upon outgassing time scales. The cyclical regimes of foam renewal and collapse were characterized in both time and frequency domains. The results obtained are discussed and compared with previous models. Finally, we present the implications of our experimental observation for volcanic eruptions, focusing particularly on gas-piston activity at lava lakes.

2. Experimental Setup

The decompression experiments were performed in a shock-tube device, consisting of a cylindrical Plexiglas autoclave serving as a high-pressure section (77.5 cm^3 volume, radius 1 cm) and a high-volume (3.7×10^5 cm^3 volume; radius 20 cm) expansion chamber operating at ambient pressure (for further details on the apparatus, see *Spina et al.* [2016b]). The samples, consisting of ~20.4 cm^3 of Newtonian silicone oils, were inserted at the bottom of the autoclave. Once mounted, we saturated the samples with Argon gas for 72 h at 10 MPa and then decompressed the system through a dedicated valve. During the slow decompression (~10^{-2} MPa s^{-1}), typically lasting roughly 1000 s, the pressure in the system was measured by two static pressure transducers, and the dynamics of the fluid was tracked using a video camera operating at 25 fps.

We selected for our study on periodicity a subset of the experiments from *Spina et al.* [2016b] (see Table 1) comprising (1) pure silicone oil samples with viscosities of 100 Pa s (#3 and #4) and 1000 Pa s (#5), both

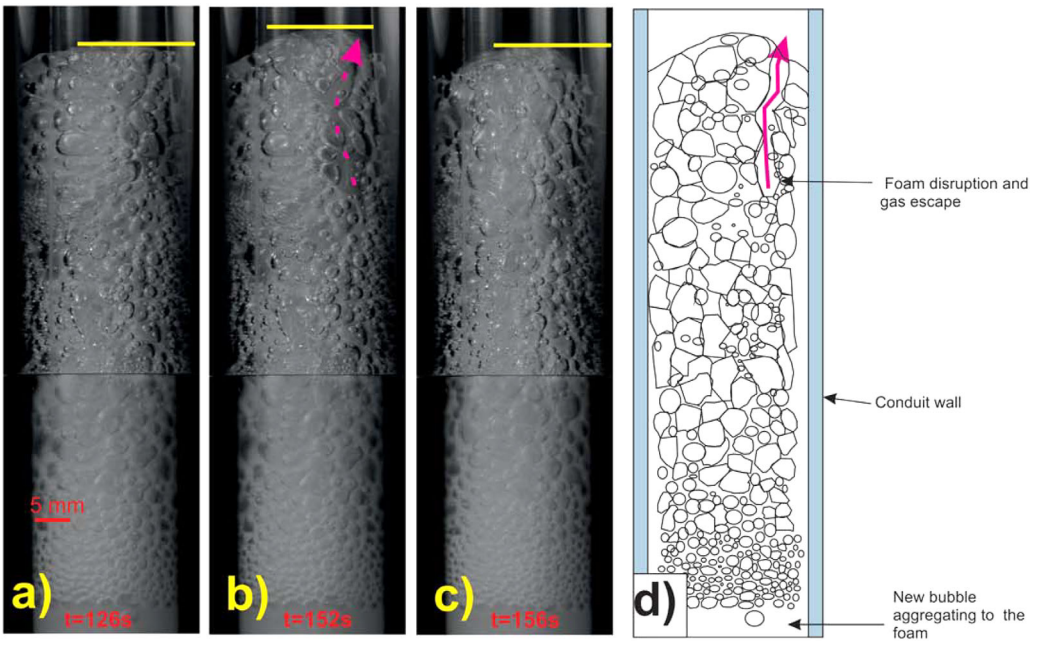

Figure 1. (a–c) Snapshots from experiment #15 (100 Pa s silicone oil with 3 vol % of elongated crystals), corresponding to 126, 152, and 156 s after the initiation of oscillation phase, respectively. The yellow line marks the position of the fluid surface. (d) Simplified sketch representing the start of a collapse phase. The disruption of the foam due to coalescence opens a pathway for gas escape, indicated both in Figures 1b and 1d by a pink arrow.

within the range of viscosity of basaltic melts [e.g., *Giordano et al*., 2004]; and (2) particle-bearing experiments with a relatively low particle volume fraction ϕ (#8 to #11 and #14 to #16) added to the 100 Pa s silicone oil basis. The particles used to mimic the role of crystals were (1) spherical glass beads (average diameter: 83 μm; aspect ratio: 1) and (2) elongated glass fibers (average length and diameter: 149 and 14 μm; aspect ratio: 10). Two experiments were added to the existing data set (#26, #27; the numbering of experiments extends that of *Spina et al*. [2016b]) both were performed on 1000 Pa s silicone oil, to ensure repeatability of observations.

According to *Mueller et al*. [2010, and references therein], for spherical particles, the diluted and semidiluted regimes are restricted to $\phi \leq 0.02$ and $\phi \leq 0.25$, respectively. Conversely, for a spheroidal particle with an aspect ratio of 10, the limits are $\phi \leq 0.005$ and $\phi \leq 0.05$, respectively. Therefore, our particle-bearing experiments were performed in the diluted regime at $\phi = 0.01$(#8) and $\phi = 0.003$(#14), for spherical and elongated particle, respectively, and in the semidiluted regime at $\phi = 0.1$, 0.2 (#9, #10) and $\phi = 0.03$, 0.07 (#15, #16) for spherical and elongated particles, respectively (Table 1).

3. Results

Upon decompression, we observed bubble nucleation and the development of a foam layer at the top of the sample. The foam expands until coalescence becomes dominant, and the mixture enters a regime of repeated periodical foam growth and outgassing (*foam oscillation regime* [*Spina et al*., 2016b]; see supporting information videos Spinaetal_ms01, −02 and −03).

In some cases, we observed the bursting of individual bubbles at the surface and/or at the contact with the conduit wall, abruptly opening a pathway for gas escape from greater depths (Figure 1). Some other collapses were unrelated to any observable burst at the surface, with coalescence occurring instead within the foam at the subsurface, followed by inward motion of the outermost sample section.

Tracking foam height is the simplest method to estimate foam stability [e.g., *Iglesias et al*., 1995]. The periodic degassing style of our mixtures was characterized by tracking the variation with time of the height of a central point along the fluid surface, together with two lateral points roughly 5 mm apart (Figures 2–5). The repetition of cycles of foam growth and collapse is reflected by well-defined oscillations at the top of the

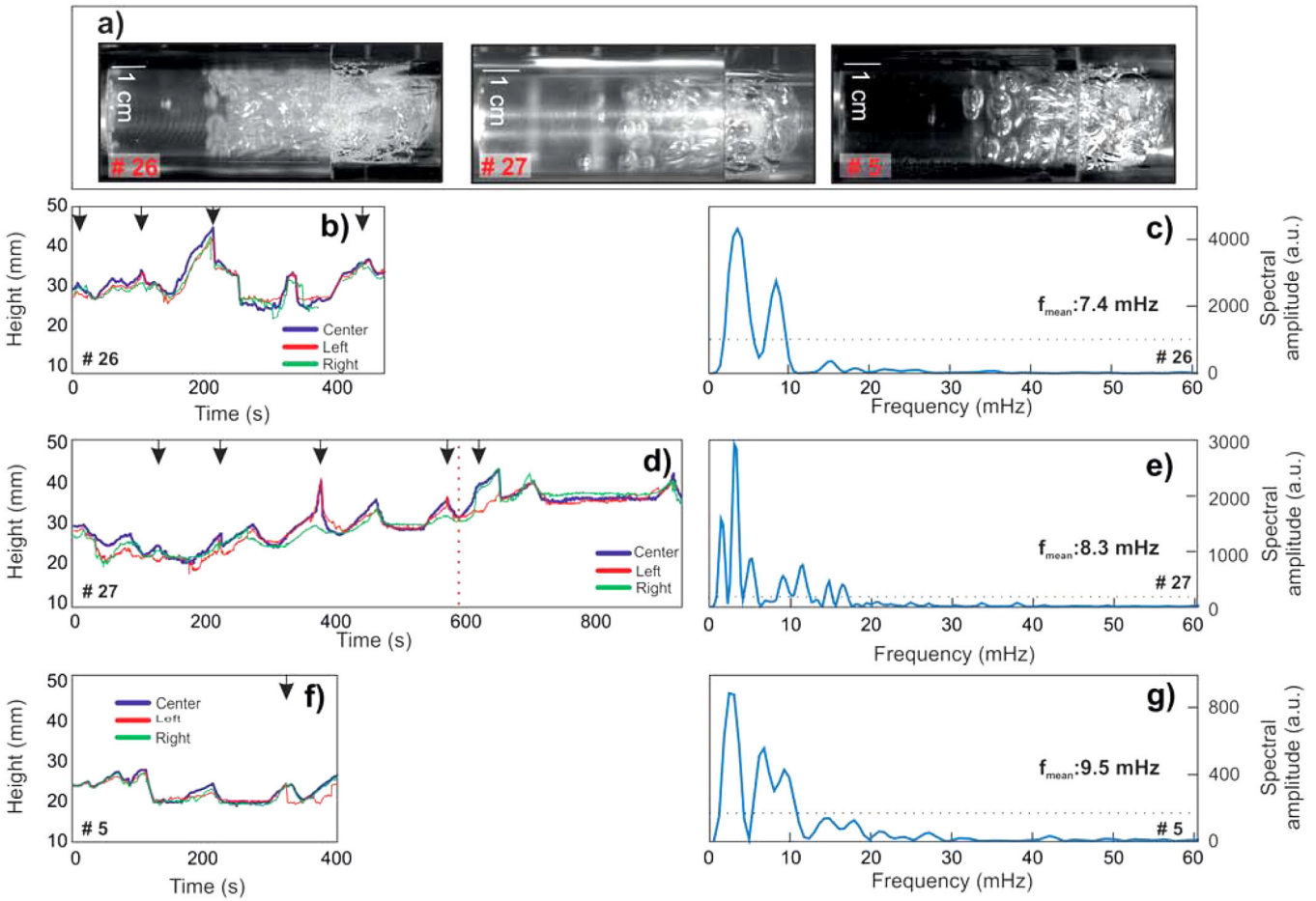

Figure 2. (a) Snapshots from experiments #26, #27, and #5 picturing the initiation of foam oscillation. (b, d, f) Height variation of the fluid surface, measured at a central point along the surface (blue line) and on two lateral point roughly 5 mm apart (red and green lines), for experiments #26, #27, and #5, respectively (silicone oils with viscosity of 1000 Pa s, particle free; see Table 1). Data were collected with a sampling rate of 2 Hz. The pink dotted line indicates the time of aggregation to the foam layer of a bubble nucleated at the base of the experimental conduit. Black arrows indicate bursting of bubbles at the surface and/or at the contact with the wall, preceding the foam outgassing. Note that time zero corresponds to the beginning of foam oscillation regime. (c, e, g) Lomb-Scargle spectrum of the height of the central point along the fluid surface (blue solid line in Figures 2b, 2d, and 2f). The grey dotted line marks a level of significance for spectral peaks equal to 95%. The mean frequency value (f_{mean}) is shown at the right bottom corner.

mixture. In order to better characterize such periodicity, we additionally performed Lomb-Scargle spectral analysis [e.g., *Lomb*, 1976; *Scargle*, 1982], based on the least squares fit of sinusoids to data samples, and particularly recommended for uneven sampled data. Experiments with particle-bearing samples occasionally contain gaps in the foam height data resulting from images where fluid level cannot be clearly identified and thus not clearly tracked (e.g., dotted lines in Figures 4 and 5 and supporting information video Spinae-tal_ms02). The obtained spectra are shown in plots c, e, and g of Figures 2, and 5, and plots c and e of Figure 3. To minimize the contribution of very low-frequency peaks (approximately <3 mHz, periods >300 s) that are not related to the foam-outgassing process, but rather to the bulk behavior of the mixture through the decompression, we evaluated for each spectrum a mean frequency as follows:

$$f_{mean} = \frac{\sum_{i=1}^{N} (pxx_i * f_i)}{\sum_{i=1}^{N} pxx_i} \quad (1)$$

where f_{mean} is the weighted mean of the overall frequency distribution, i.e., a kind of center of mass (COM) of the spectrum [*Carniel et al.*, 2005], and pxx_i represents the power spectral density of the signal evaluated at each of the N frequency f_i.

Particle-free experiments are illustrated in Figures 2 and 3. Experiments #5, #26, and #27 (1000 Pa s) display a more regular oscillatory trend and higher amplitudes compared to experiments #3 and #4 (100 Pa s). In

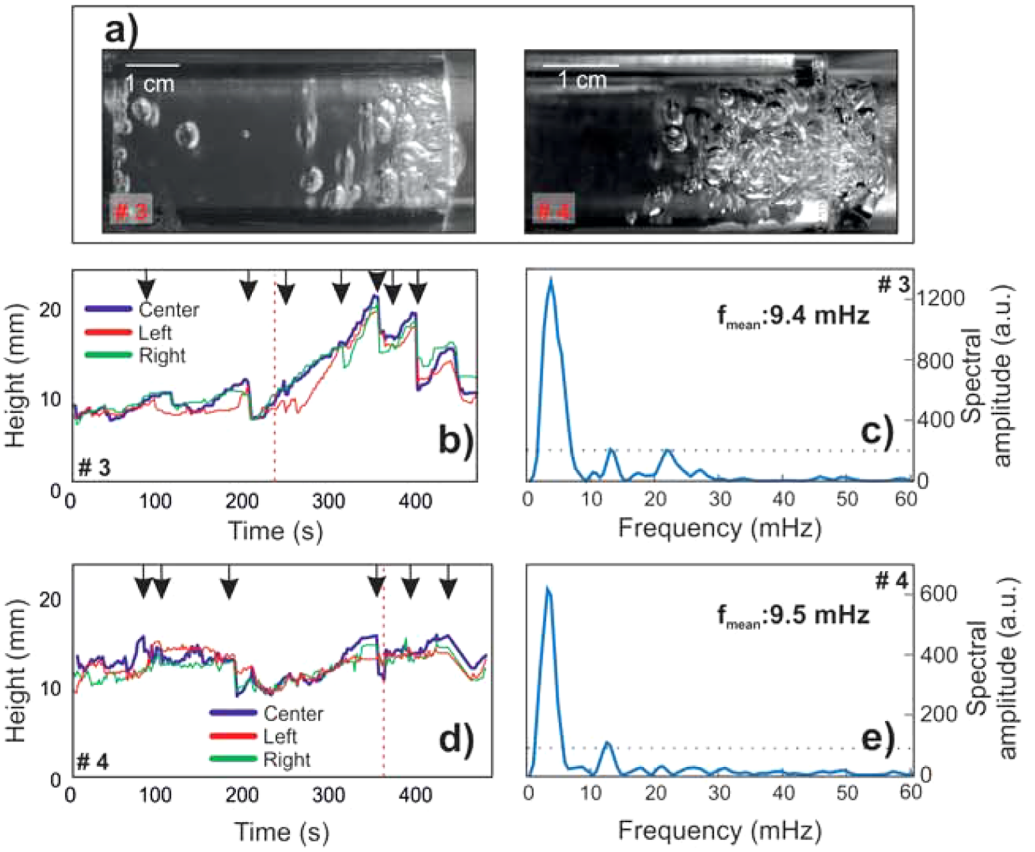

Figure 3. (a) Snapshots from experiments #3 and #4 picturing the initiation of foam oscillation. (b, d) Height variation of the fluid surface, measured on a central point along the surface (blue line) and on two lateral point roughly 5 mm apart (red and green lines), for experiments #3 and #4, respectively (silicone oils with viscosity of 100 Pa, particle free, see Table 1). (c, e) Lomb-Scargle spectrum of the height of the central point along the fluid surface (blue solid line in Figures 3b and 3d). Other symbols and sampling rate as in Figure 2.

the latter, due to the more rapid dynamics of volatile transport in the lower-viscosity fluid, a thinner foam layer is developed. The mean frequency of the 1000 Pa s samples lies in the range 7.4–9.5 mHz (equivalent to periods of 135–105 s). Experiments #3 and #4 have a very coherent spectrum with mean frequency at values of about 9.5 mHz (105 s).

The results from spherical and elongated particle-bearing experiments are shown in Figures 4 and 5, respectively. Note that the spectra become broader with increasing solid content, and peaks at frequencies higher than 20 mHz appear (e.g., Figures 4e, 4g, and 5e). Concomitantly, the mean frequency increases from the value of ∼8 mHz (i.e., periods of 125 s) in #8 and 14 (i.e., diluted regime) to the range of 12–17 mHz (i.e., periods of ∼83–60 s) in #9, #10, #14, and #15 (i.e., semidiluted regime). Furthermore, for experiments #9 and #10, the growth and collapse time scale increases with elapsed time (Figures 4d and 4f). An analogous but less pronounced tendency to an increase in the time scale is observed in #8 (Figure 4b). Similarly, experiments #15 and #16 display longer oscillation time scales at later stages (Figures 5d and 5f).

In Figure 6a, the duration of several cycles of growth and outgassing, measured from the curves shown in Figures 2–5, is plotted versus the viscosity of the sample. The measured cycle duration ranges between 15 and ∼90 s for experiments #3 and #4 and between 15 and 120 s for experiments #5, #26, and #27, consistent with the spectral observations. In the pure silicone oils, at different viscosities, no relevant variations of time scale or amplitude of the cycles were observed during the duration of the investigation (roughly 900–1000 s). On the contrary, as noted above, semidiluted particle-bearing experiments exhibit an increase in the cycle duration with time (Figures 4 and 5). This increase is further highlighted by the roughly linear relationship between the duration of each cycle and its starting time along the decompression (Figure 6b). Thus, the high values of the dotted box in Figure 6a represent measurements obtained at a later stage of decompression (roughly after 400 s from the beginning of the foam oscillation regime). If we neglect these

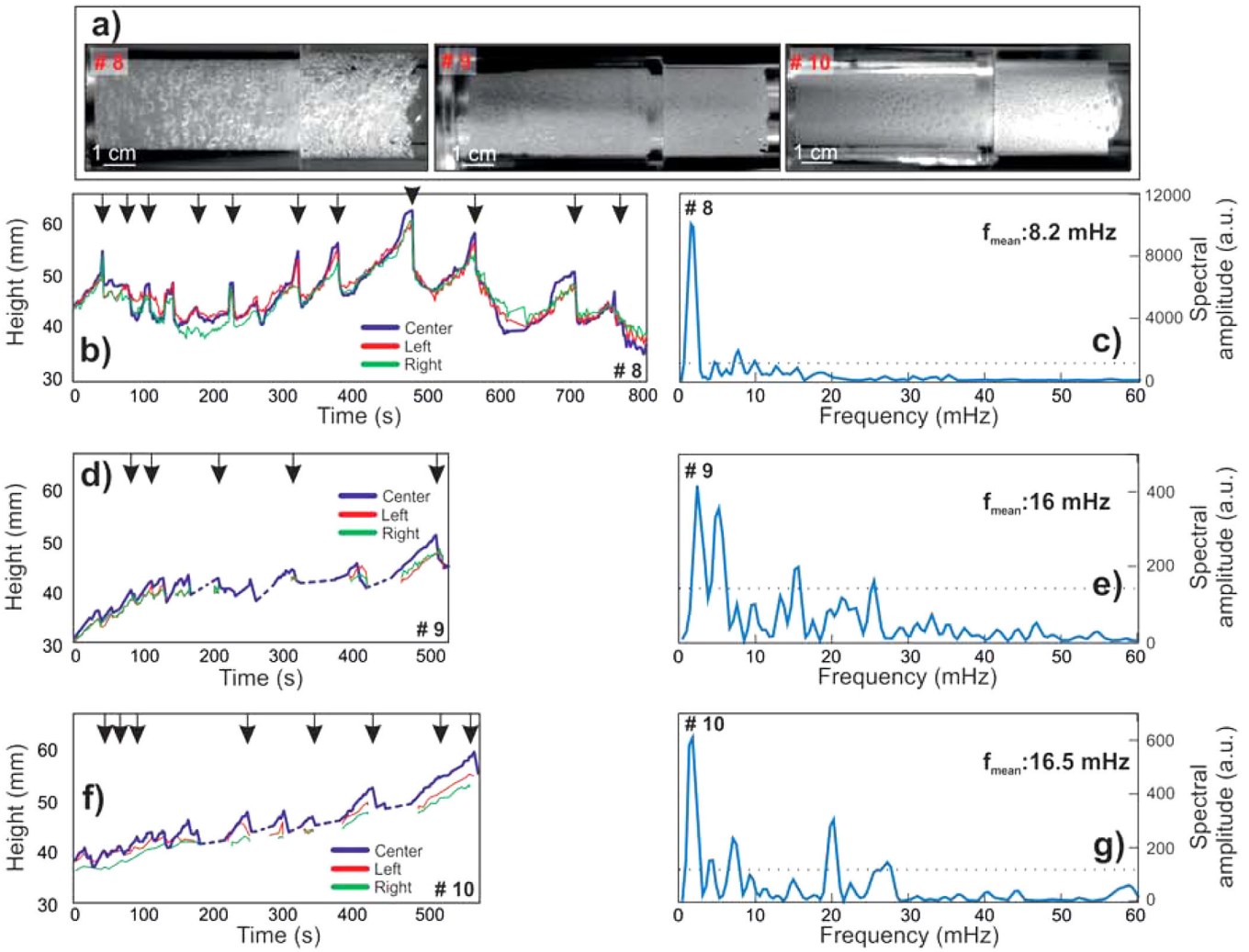

Figure 4. (a) Snapshots from experiments #8, #9, and #10 picturing the initiation of foam oscillation. (b, d, f) Height variation of the fluid surface, measured on a central point along the surface (blue line) and on two lateral point roughly 5 mm apart (red and green lines), for experiments #8, #9, and #10, respectively (silicone oils with viscosity of 100 Pa s, and volume percentages of spherical crystals of 1, 10, and 20%, respectively, as shown in Table 1). (c, e, g) Lomb-Scargle spectrum of the height of the central point along the fluid surface (blue solid line in Figures 4b, 4d, and 4f). Other symbols and sampling rate as in Figure 2.

high values and compare results for experiments at times $<$400 s, the overall decrease in cycle duration with an increase in viscosity (i.e., particle content) becomes evident for particle-bearing samples (see section 4 for further discussion).

In Figure 6c, we plotted the growth phases of 34 oscillations, picked at different times from all the experiments, and selected by ensuring that the signal is representative of the bulk mixture and not related to individual bubbles on the fluid surface. In most cases, foam growth was characterized by a decelerating pattern of the fluid level rise.

4. Discussion

4.1. Comparison of the Time Scales of Foam Stability With Previous Investigations

In the present experiments, we observed the repeated spontaneous partial disruption of the analogue foam at the top of the fluid column, often preceded by the arrival and bursting of bigger bubbles at the surface, opening an escape pathway for the gas phase (see Figures 1 and 7 and supporting information videos). This is consistent with the fact that foams are metastable systems, spontaneously tending to separate into two distinct bulk phases, with different dynamical time scales [*Bhakta and Ruckenstein*, 1997]. At later stages,

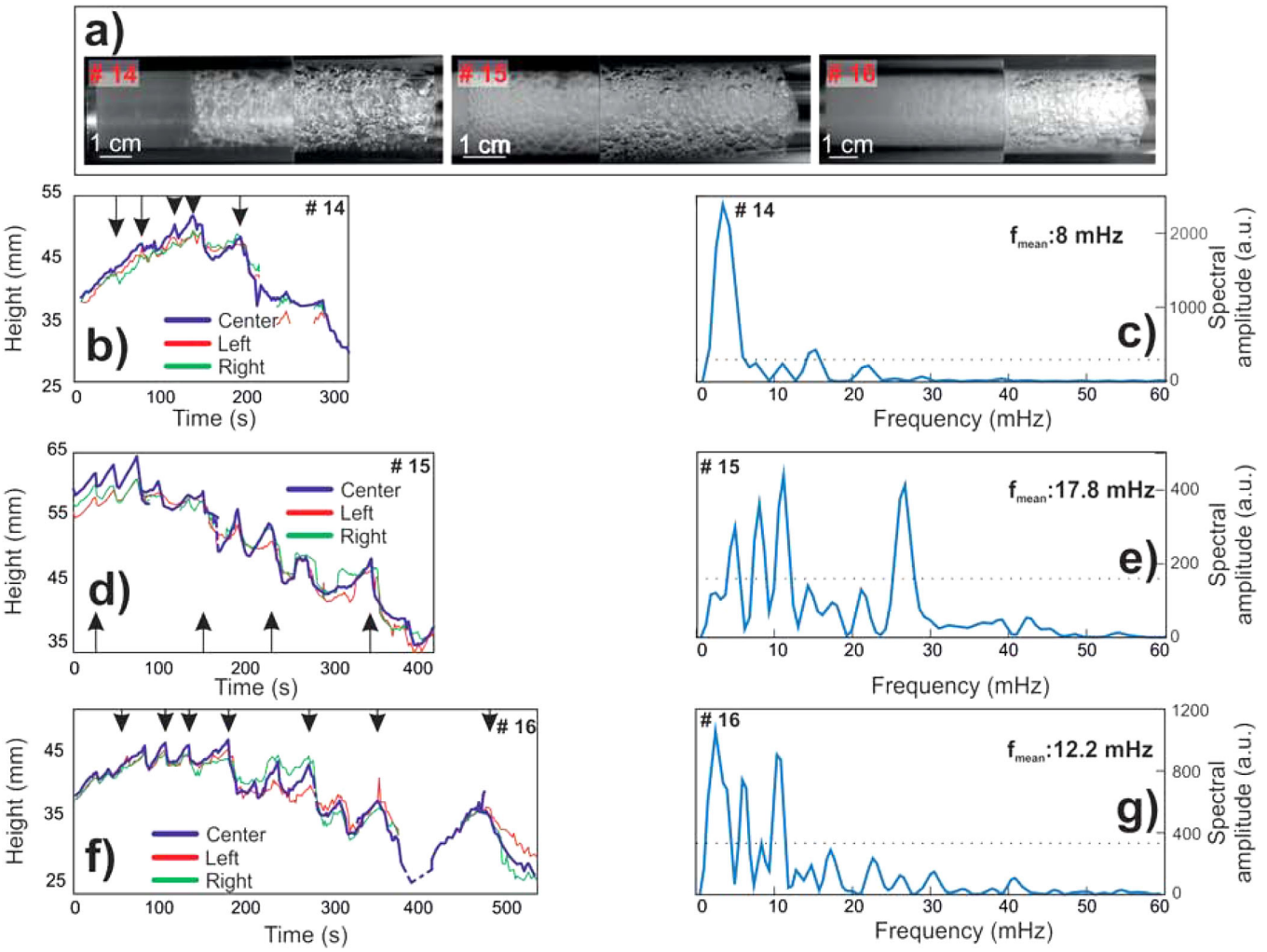

Figure 5. (a) Snapshots from experiments #14, #15, and #16 picturing the initiation of foam oscillation. (b, d, f) Height variation of the fluid surface, measured on a central point along the surface (blue line) and on two lateral point roughly 5 mm apart (red and green lines), for experiments #14, #15, and #16, respectively (silicone oils with viscosity of 100 Pa s, and volume percentages of elongated crystals of 0.3, 3, and 7%, respectively, as shown in Table 1). (c, e, g) Lomb-Scargle spectrum of the height of the central point along the fluid surface (blue solid line in Figures 5b, 5d, and 5f). Other symbols and sampling rate as in Figure 2.

bubbles, originating within the liquid, contribute to the growth of the foam layer gathering at the liquid-foam interface at the bottom of the foam column. In a similar way, the foam accumulates at the top of the fluid column within the conduit and acts as a rheological barrier against the ascent of individual bubbles toward the surface [e.g., *Dibble*, 1972; *Chouet and Dawson*, 2015].

As noted above, *Jaupart and Vergniolle* [1989] experimentally analyzed the periodical collapse of a foam in a cylindrical tank topped by a vertical thin conduit, using silicone oils and glycerol solution as analogue materials, and injecting gas flux of up to 2000 cm^3/min. They observed that collapse occurs at a critical thickness, related to (1) the fluid viscosity and (2) the input gas flux, which induces maximum deformation of the bubbles in contact with the roof. In our experiments, there is no upper constriction to foam expansion, and collapses appear related to the topological rearrangement/internal evolution of the foam structure rather than to the achievement of a critical thickness.

According to *Nguyen et al.* [2013, and references therein], several mechanisms contribute to the film thinning at the base of the foam collapse, namely (i) gravitational forces; (ii) capillary forces; (iii) bubble growth (either by decompression or diffusion); (iv) foam shearing, by magma ascent or by bubble coalescence. The liquid expulsion (i.e., drainage) by gravity and/or capillary forces provide a lower bound on coalescence rate; hence, several models have been developed to study the drainage times of individual films. Among

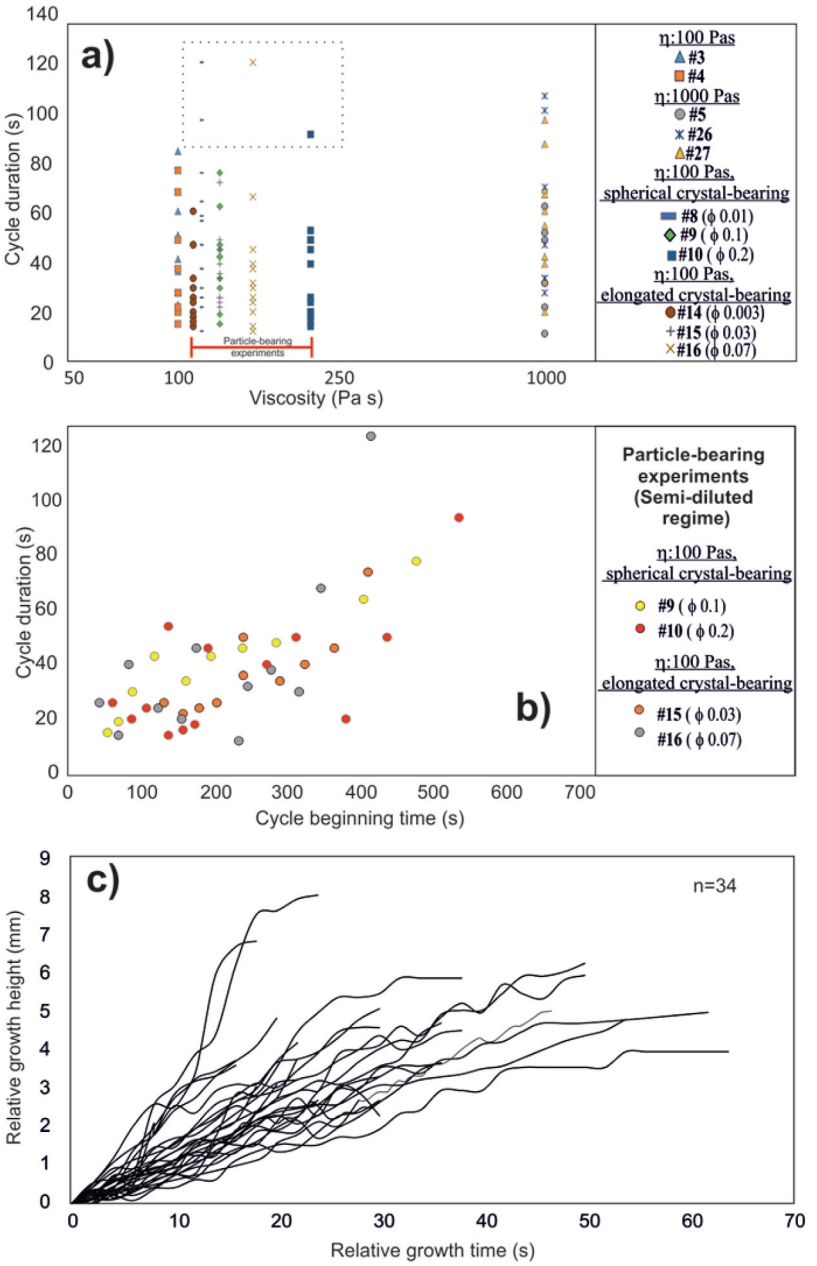

Figure 6. (a) Duration of growth-and-collapse cycles versus sample viscosity. Data points enclosed in the dotted box were measured at later stage (> 400 s approximately from the initiation of oscillation phase) of the experiments. (b) Duration of growth-and-fall cycle of the semidiluted particle-bearing experiments plotted against the time at which the cycle begins. Note that time zero correspond to the beginning of foam oscillation regime. (c) Height variation of a central point along the fluid surface, measured during the growth phase of 34 cycles, relative to the height of the mixture at the beginning of the same cycle. A linear or decreasing trend of the surface uplift is evident.

them, *Proussevitch et al.* [1993] analyzed the process of liquid expulsion along a film (between two bubbles) and a Plateau border (between three or more bubbles), focusing on the case of bubbles in equilibrium with the melt (no diffusive or decompressive growth) and dominated by capillary forces. Successively *Nguyen et al.* [2013] revised the classic formulation based on the assumption of no-slip boundaries at either side of the liquid film, taking into account the possibility of mobile film interfaces (in the absence of surfactants or impurities). They verified their theory experimentally on air bubbles injected into silicone oil, and rising to the air-liquid interface. Although *Nguyen et al.* [2013] investigated a single bubble at the surface of a large-volume liquid, in case of negligible external deformation/bubble growth their experiments represents a first-order analogue to inter-bubble film drainage in vesicular magmas, given that the overall force balance

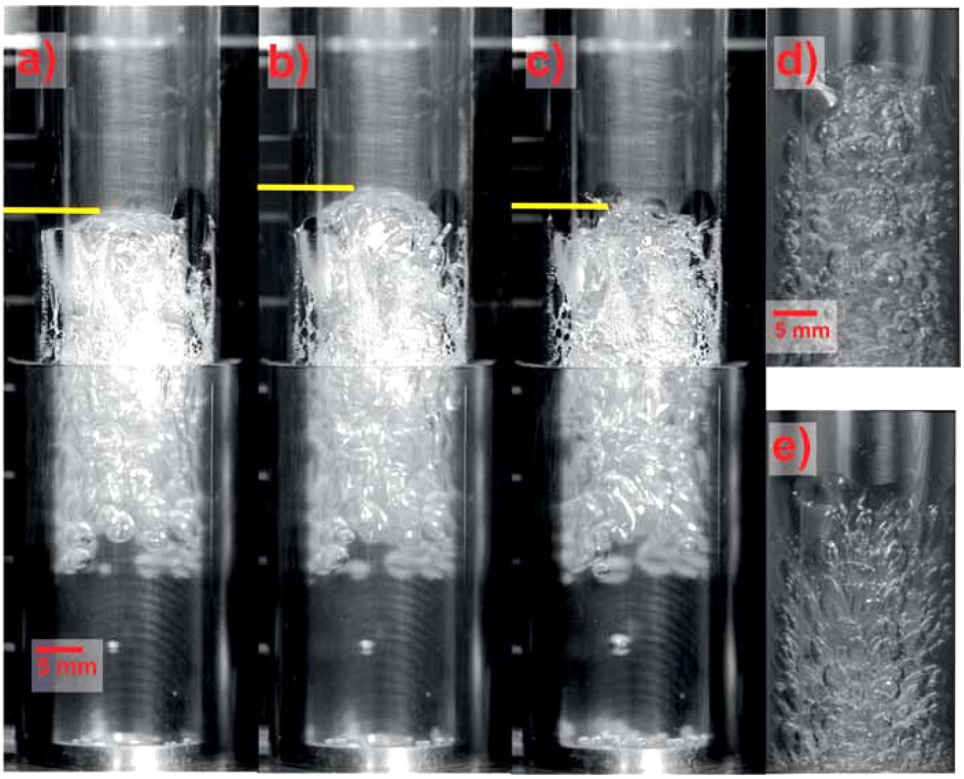

Figure 7. (a–c) Snapshots from experiments #27 (1000 Pa s) and (d, e) #14 (100 Pa s with 0.3 vol % of elongated crystals), picturing the growth and disruption of the outermost portion of the foam. The inward flow of the collapsing upper portion of the foam is evident in Figure 7e.

remains unaffected. As such, the results of their study are proposed as a basis against experiments involving multiple or growing bubbles, as considered in this work, and represent the most appropriate starting point to assess the effect of complex dynamic conditions.

To determine whether capillary or gravity forces control drainage process, a parameter, i.e., here the capillary length, is computed according to the following [i.e., *Nguyen et al*., 2013]:

$$\lambda = \sqrt{\sigma/\Delta\rho g} \tag{2}$$

where σ is the surface tension, $\Delta\rho$ is the density difference between the bubble and the surrounding liquid, and g the acceleration due to gravity. For bubble radii smaller than λ, capillary forces dominate, whereas in the opposite case, gravity forces prevail. In our experiments, σ and $\Delta\rho$ correspond to 0.0215 N m^{-1} and 968.3 kg m^{-3}, respectively, yielding λ equal to 1.5 mm, which is close to the value defined for silicate melts (3 mm) [*Proussevitch et al*., 1993]. Thus, given the observed distribution of bubble radii (on the order of $<$1–4 mm), both regimes are taken into account. In *Nguyen et al*. [2013], the gravitational (t_g) and capillary (t_c) drainage times of individual viscous bubbles are computed according to the following equations

$$t_g = C_g \ln\left(\frac{\delta_0}{\delta_f}\right)\frac{\eta}{\Delta\varrho g R} \tag{3}$$

$$t_c = C_c \ln\left(\frac{\delta_0}{\delta_f}\right)\frac{\eta R}{\sigma} \tag{4}$$

with η fluid viscosity, σ is the surface tension, δ_0 and δ_f are the initial and the final film thickness, respectively, R is the bubble radius, and C_g and C_c are empirical constants. The values of C_g, C_c, and $ln(\delta_0/\delta_f)$ for silicone oils were experimentally investigated by *Nguyen et al*. [2013] and correspond to 5, 20, and 7.

Figures 8a and 8b show the results expected for our analogue samples at different viscosities and bubble radii, according to the above mentioned drainage-dominated model. Given that equations (3) and (4) do

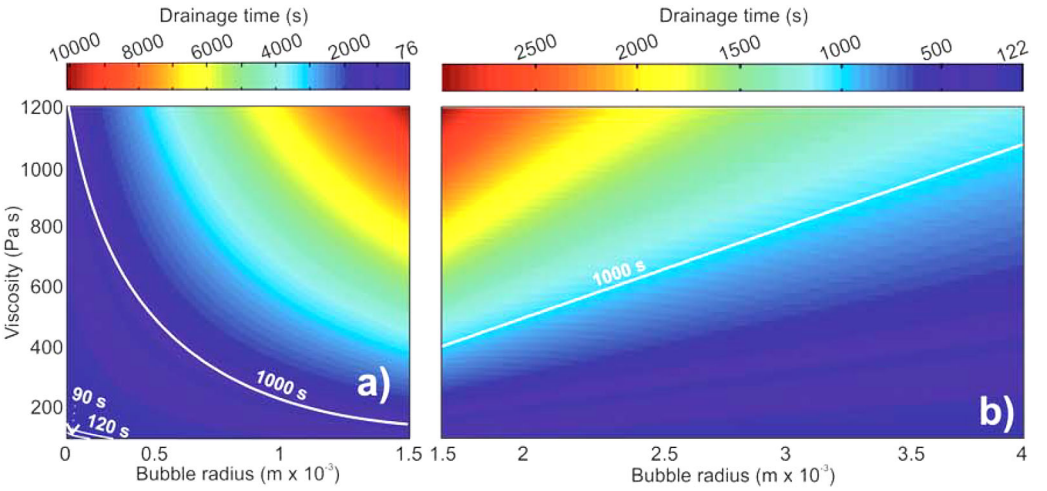

Figure 8. (a) Capillary and (b) gravity drainage time computed for silicone oil at different bubble radii and liquid viscosity from *Nguyen et al.* [2013]. We fixed $\sigma = 0.0215$ N/m; ln $(\delta_0/\delta_f) = 7$; $\Delta\rho = 968.3$; $C_c = 20$, $C_g = 5$ (for more details see section 4.1). In Figure 8a, the white solid lines mark the values of liquid viscosities and bubble radii required for drainage times equal to 90 s (maximum value for experiments #3, #4), 120 s (maximum value for experiments #5, #26, and #27), and 1000 s (as a reference for drainage times $\approx$ 1 order of magnitude bigger than observed).

not account for the role of particles, we compare these models with our results from pure silicone oil experiments. As evident from Figures 8a and 8b, foam disruption time scales are systematically overestimated from equations (3) and (4) by up to more than 1 order of magnitude, exemplified by the high-viscosity experiments #5, #26, and #27. This misfit emanates from the bubble growth effects and the shear rate within the conduit, and clearly remarks that such contribution cannot be neglected in situations where dynamic conditions prevail.

4.2. The Effect of Shear Deformation and Bubble Growth on Film Thinning

Okumura et al. [2008] performed experiments on rhyolitic obsidian, observing an increase in the degree of bubble coalescence and breakup with shear strain for strain rates from 0.017 to 0.027 s^{-1}. In our experiments, shear strain rates γ related to the vertical flow ascent in the conduit were evaluated by using $\gamma = 4u_0/3R_c$, where u_0 is the axial velocity and R_c the conduit radius [e.g., *Llewellin and Manga*, 2005]. The axial ascent velocity was estimated from the profile of the fluid surface. In order to estimate an average value, a complete analysis would require the computation of the shear strain rate at several depths along the conduit [*Llewellin and Manga*, 2005]. Our interest however focuses specifically on the uppermost section of the foam, where coalescence sets the time scale of collapse. We obtained strain rates on the order of 10^{-3} s^{-1} for 100 Pa s experiments and 10^{-2} s^{-1} for experiments with viscosities of 1000 Pa s as well as for particle-bearing experiments. Assuming a range of bubbles radius on the order of 0.05–4 mm, the bubble shape relaxation time (i.e., time for bubbles to recover their spherical shape upon cessation of shear stress), computed as $\tau = R\eta/\sigma$, is in the range of 2–160 s for viscosities of 1000 Pa s, and decreases to only 0.2–16 s in samples with viscosities of 100 Pa s. Accordingly, we assume that during the vertical ascent in experiments #5, #26, and #27, bubbles might have experienced shear deformation. This hypothesis is confirmed by video observations depicting evident bubble elongation due to shear in these samples (Figures 7a–7c, and supporting information video Spinaetal_ms01). Therefore, we conclude that a shear strain rate in the order of 10^{-2} s^{-1} favored coalescence in the experiments #5, #26, and #27; here bubbles were stretched during fluid ascent, which is in agreement with *Okumura et al.* [2008] and explains the maximum deviation observed for these samples from the models previously discussed.

Additionally, measurements of the expansion rate in particle-free experiments (#3 to #5 and #26, #27) suggest that bubbles at the base of the foam layer have a growth rate of 10^{-2}–10^{-1} mm/s. Bubble growth related to both decompression and/or diffusion produces an increase in bubble radius and local porosity, thereby decreasing the time scale for disruption. Notably, *Gardner* [2007] found an increase in coalescence episodes upon isothermal decompression, which underpins a dependence of coalescence on the decompression state of the system.

Our experimental results suggest that the time scale for outgassing measured upon dynamic conditions are up to 1 order of magnitude smaller than the theoretical times estimated for static conditions. Similar results were obtained by *Neethling et al*. [2005], who studied the film stability of sodium dodecyl sulphate (SDS) foams. They found that the pressure required to overcome bubble-disjoining pressure was smaller than expected from single film measurements, and attributed this evidence to vibration due to bubble bursting, topological rearrangements of bubbles and to effects related to the flow of the mixture. *Neethling et al*. [2005] consequently assumed a distribution of bursting probabilities to be more representative of real foams than a narrow range of values. Together with our experimental results, such evidence highlights the urgency for future investigations to focus on realistic models of film stability taking into account flowing/decompressed foams.

4.3. The Influence of Particles on Foam Dynamics

In our experiments, the presence of particles plays a fundamental role, enhancing a more pervasive bubble distribution than in pure silicone oils and a higher gas-volume fraction due to heterogeneous nucleation [*Spina et al*., 2016b] (Table 1: #8 to #16 versus #3, #4). The marked increase in volatile content can therefore be described as an increase in hypothetical gas flux from the bubbly fluid below the foam. This is reflected in the overall trend of the foam height through time (Figures 4 and 5): at high gas flux, the upward velocity of the gas phase exceeds the downward flux due to liquid drainage, and foam height increases indefinitely [e.g., *Grassia et al*., 2006], as observed in #9, #10, whereas in #3, #4, #5, and #8 we noted a constant trend, i.e., rate of bursting close to the surface matches the gas rate from below [*Neethling et al*., 2005]. Conversely, the decaying trend in particle-bearing experiments was attributed to a much more effective degassing related to flocculation or particle reorientation [*Spina et al*., 2016b]. Such upward or downward movement of the bulk mixture was removed from the signal before measuring the time scale of foam collapse.

Differences in crystal content in our experiments correspond to different bubble size distributions and gas volume ratio in the liquid. In particle-bearing experiments, the radii of bubbles within the foam are smaller than in particle-free experiments (Table 1), and therefore a faster drainage time of the films is expected [*Grassia et al*., 2006]. Furthermore, the presence of particles provokes increased bubble breakup by the solid network and coalescence [*Mena et al*., 2005], therefore decreasing the time scale for outgassing. Previous studies performed on particle-rich analogue mixtures show that the gas phase tends to deform around the areas that offer larger resistance [*Oppenheimer et al*., 2015], creating tortuous and complex paths for gas escape and promoting the development of a permeable network. Indeed, in our experiments, the frequency of outgassing increases (increasing bursting rate) with particle content, as evident from the mean frequency (Figures 4 and 5). In particular, the mean frequency is doubled in the semidiluted regime when compared to the diluted regime, both for spherical and elongated particle-bearing experiments. Within the semidiluted regime, we did not observe a primary role of the amount of solid loading.

Additionally, we observed in particle-bearing experiments a general tendency to a lengthening of the oscillation time scale with elapsed time in the semidiluted regime (Figure 6b). We attribute this evidence to the disruption of the most external foam layer, producing an increase in the film thickness of the underlying foam, thus doubling the collapse time scale [*Proussevitch et al*., 1993]. With time, drainage redistributes the liquid within the foam, progressively drying the outermost foam layer, which becomes again unstable [*Bhakta and Ruckenstein*, 1997]. Interestingly, we did not observe the same temporal evolution for particle-free experiments. We infer that the presence of particles reduces the speed of fluid redistribution enhancing the effect played by the increase in film thickness at later stages of the foam evolution.

4.4. Implications for Natural Systems

The applicability of our experiments to the dynamics of volatiles in shallow basaltic systems has been previously verified at low gas volume fraction ($\phi_b < 0.45$; i.e., before the development of the foam) for each experiment performed in the diluted regime by means of nondimensional numbers, e.g., Reynold, Eötvos, Morton bubble numbers, and Capillary numbers [*Spina et al*., 2016b, and references therein]. This approach ensures the similarity in the balance of forces (e.g., inertial, viscous, surface tension, buoyancy, and capillary forces) acting on each fluid volume in the experimental and natural cases which are extensively discussed in *Spina et al*. [2016b].

Table 2. Comparison of Nondimensional Numbers to Compare Drainage Time Scales in Experimental and Natural System (Pi-Groups Analysis)[a]

Nondimensional Parameter	Experimental Value	Volcano-Scale Condition
$\Pi(1)=R/\delta_f$	10^3-10^4	10–10^{4b}
$\Pi(2)=\delta_0/\delta_f$	10–10^3	10–10^{3b}
$\Pi(3)=\delta_f\eta/\sigma$	10^1-10^3	10^3-10^{4b}

[a]Parameter list: R = bubble radius, δ_0 = initial film thickness; δ_f = critical film thickness; η = fluid viscosity; σ = surface tension.
[b]R, δ_f, and δ_0 from *Carey et al.* [2012].

For higher gas volume fraction ($\phi \gg 0.45$, i.e., the foam stage discussed in this study), a few additional considerations are necessary. Foams are metastable time-varying systems, with short-scale longitudinal and radial variations and for which no rheological models are yet defined [e.g., *Mader et al.*, 2013]. Therefore, we focused on the foam drainage process, to define an appropriate set of nondimensional parameters rather than comparing the overall properties of the systems. Assuming the same value of gas volume ratio ε and gravity constant g both in the experiment and in a basaltic system, the drainage time due to capillary or gravity forces, t, depends on the following significant variables (already defined in section 4.1):

$$t=f\{\delta_f,\ \delta_0, R,\ \sigma,\ \Delta\rho, \eta\} \tag{5}$$

The above mentioned parameters involve three fundamental dimensions (mass, length, and time), from which we derive the three following nondimensional Pi-groups by Buckingham-Pi theorem [*Buckingham*, 1914]:

$$\Pi(1) = \mathrm{R}/\delta_\mathrm{f} \tag{6}$$

$$\Pi(2) = \delta_0/\delta_\mathrm{f} \tag{7}$$

$$\Pi(3) = (\delta_\mathrm{f} * \eta)/\sigma \tag{8}$$

As reference for a basaltic magma, we took values of δ_f, σ, and η equal to 0.1 μm, 0.3 N m^{-1}, and 100–1000 Pa s [e.g., *Carey et al.*, 2012; *Giordano et al.*, 2004]. Similarly, for silicone oil, δ_f is equal to 0.1 μm [e.g., *Nguyen et al.*, 2013], σ correspond to 0.0215 N m^{-1}, and η is either 100 or 1000 Pa s. Bubble radius is difficult to constrain, especially for natural systems where measurements can span several orders of magnitude. Here we here assume a range of radii in the order of 5 μm to 5 mm for basaltic magma [*Carey et al.*, 2012], and 0.05–4 mm for experimental observations, where the lower boundary of the range is determined by capability of visual detection. The resulting values are reported in Table 2. We observe a good fit for $\Pi(1)$ and $\Pi(2)$, while $\Pi(3)$ for our experiment is about 1 order of magnitude smaller than in volcanic systems. This difference is likely related to the major role played by surface tension in liquid drainage in basaltic volcanoes that can imply—for the same viscosity—longer collapse time than observed here when dealing with systems dominated by capillary drainage. The effect of surface tension can be neglected for systems dominated by gravity drainage (bubble radius on the order of 1 cm) [*Proussevitch et al.*, 1993]. The substantial similarity in the two systems suggests that the analogue foam is able to reproduce the dynamics of magmatic foams. Nevertheless, it is important to remind that the range of variability of parameters (as for instance the bubble radius) is much wider in nature than in our experimental systems. For the same experimental conditions, each of our experiments takes into account exclusively a single decompression rate, and no variations in the gas flux were allowed. Both conditions might produce important changes in the evolution of periodicity. Therefore, we do not aim to pinpoint a specific time scale for basaltic systems, but rather to define the physical processes and the effects played by dynamic conditions on the periodicity of outgassing.

In particle-bearing experiments, the relative size of particles affects the style of gas-solid interaction. In order to parametrize this geometrical factor; we computed ψ, i.e., the ratio between bubble diameter and particle width [*Belien et al.*, 2010; *Spina et al.*, 2016b]. For spherical particle-bearing experiments (particle width: 83 μm) with bubble radii of 0.3–1.7 mm, ψ is equal to 7–40. For elongated particle-bearing experiments (particle width: 149 μm), we obtained a value of ψ equal to 2–32 over a bubble radius range of 0.2–2.4 mm. Therefore, assuming a population of crystal of 100 μm, for both particle shapes, our results are applicable to bubbles with radii of hundreds of millimicrons to few millimeters. The preliminary results presented here for particle-bearing experiments underline the urgency for future research to explore a wider range of geometrical factors, addressing the effects of different particle dimension on the time scale of foam outgassing.

In a shallow conduit, the growth of bubbles is dominated by decompression rather than by diffusion [*Sparks*, 1978]. Therefore, our laboratory experiments, where decompression prevails, are fundamental to target the shallow feeding system. Here the investigated decompression rates (~0.02 MPa/s), are coherent with the values for effusive-explosive eruptions (20–200 Pa s^{-1}, 2 $\times 10^4$ Pa s^{-1}) predicted by *Namiki and Manga* [2006], and with the decompression rate <0.02 MPa s^{-1} expected in natural systems, depending on their eruptive style [*Fiege et al*., 2014, and references therein].

The analysis of bubble shape in pyroclastic obsidian revealed strain rates on the order of 10^{-2} s^{-1} near the conduit wall [*Rust et al*., 2003]. *Mangan et al*. [2015] estimated strain rates of 0.03–3 s^{-1} for low-energy effusive activity and 2–425 s^{-1} for high-energy lava fountains based on the average flow velocity (0.1–320 m/s; derived from eruptive fluxes) in a conduit of 0.5–2.5 m. Based on theoretical models, *Gonnermann and Manga* [2003] suggested strain rates of 1 s^{-1} immediately prior to fragmentation. Therefore, strain rates of $<10^{-2}$ s^{-1} can be considered to reasonably simulate low-energy explosive/effusive activity within the volcanic conduit.

5. Foam Oscillation and Gas-Piston Activity at Lava Lakes

Lava lakes are usually characterized by a wide range of variations in the surface level, which can be distinguished in long-term (days to weeks) and short-term (minutes to hours) fluctuations. The former is generally related to major changes in the course of an eruption [*Tilling*, 1987]. Among short-term fluctuations, gas-piston activity is a well-known modality of degassing, originally defined to describe the cyclic rise and fall of the magma column observed during the 1969–1971 activity of Mauna Ulu vent at Kilauea Volcano (Hawaii) [i.e., *Swanson et al*., 1979]. At that time, the lava column—capped by a solidified but flexible crust—rose from few meters up to several tens of meters in 15–20 min and successively withdraws to its starting level in 1–2 min [*Swanson et al*., 1979]. *Patrick et al*. [2014] observed a maximum increase of lava lake level at Halema' uma' u crater (Kilauea Volcano, Hawaii) of 15 m in few minutes to several hours. *Marchetti and Harris* [2008] provided a detailed description of different features (thermal amplitude, occurrence, and thermal waveforms) of gas-piston activity at Pu'u 'Ō'ō crater (Kilauea) in 2001–2003. By analyzing a collection of ~4000 events, they defined the existence of repeatable thermal waveforms, and the presence of systematic changes in their type, duration and recurrence. Finally, *Orr and Rea* [2012] characterized gas pistons occurring at Drainhole vent (Pu'u 'Ō'ō crater, Kilauea) in June 2006. They reported a height increase of the lava surface of 0.7–5.3 m in a time span of 2–60 min (average value: 13 min) and an average duration of the collapse phase equal to 49 s. At that time, the vent diameter was equal to 5 m.

Several hypothesis have been advanced to explain the source of gas-piston activity. We here refer to the classification of *Patrick et al*. [2016] suggesting three main classes of source models:

1. The first class assume the existence of a shallow gas accumulation zone within the vent, either trapped by the cool superficial crust [*Swanson et al*., 1979] at the lake surface or by the underlying hot viscoelastic magma layer [*Patrick et al*., 2011]. Alternatively, the episodic growth and failure of the foam accumulated at the top of the magmatic column is inferred to occur irrespectively of the presence of a surface crust. In such a case, the foam is assumed to act as a rheological barrier [*Dibble*, 1972; *Orr and Rea*, 2012; *Chouet and Dawson*, 2015].
2. In an opposite way, the periodical ascent of deep-sourced slugs, forming from the collapse of magmatic foam at the roof of the magma chamber [i.e., *Jaupart and Vergniolle*, 1988; *Johnson et al*., 2005; *Edmonds and Gerlach*, 2007] has been proposed as source for gas-piston events.
3. Finally, *Witham et al*. [2006] suggested a model based on dynamic pressure balance, assuming that the continuous streaming of gas, and the consequent reduction of bulk density, might cause repeated collapse of the system.

Orr and Rea [2012] observe that a dynamic pressure balance model (3) implies continuous bursting of bubbles at the lava surface during magma rise that is inconsistent with field observations. Additionally, although thermal data could not discriminate between the classes of models (1) and (2) [*Marchetti and Harris*, 2008], *Orr and Rea* [2012] pointed out that the linear or decreasing rise speed of the surface level, observed in the field, is not compatible with the ascent of individual slugs toward the surface (models 2). A shallow origin for the gas source is also proposed by *Patrick et al*. [2016] based on seismic and infrasonic

observations and on the evidences of shallowly rooted spattering activity and rock fall-triggered gas-piston events. Contrary to *Edmonds and Gerlach* [2007], FTIR data from *Patrick et al*. [2016] show no CO_2 enrichment relative to other gas phases as expected for deeply sourced gas slugs.

Our experiments provide evidence that analogue magmatic foam, upon relatively low decompression rates ($<$0.02 MPa s^{-1}), spontaneously produces cyclic oscillations of the surface level due to repeated foam growth and outgassing in the conduit. This evidence contributes in assessing the importance of models based on the shallow gas accumulation zone (1) as source mechanism for gas pistons. As previously stated by *Dibble* [1972], the foam represents a rheological barrier, which inhibits direct outgassing, acting as a viscous plug. Within the foam, critically stable equilibrium is achieved in response to the different ongoing physical phenomena as growth, coalescence, rise of bubbles and liquid drainage. When collapse occurs below the surface layer, the abrupt decrease of pressure induces an inward flow of the foam (i.e., Figure 7e). The sudden decrease of pressure and gas release is in accordance with discrete jetting events observed in thermal signals [i.e., *Johnson et al*., 2005], previously interpreted as the results of slugs penetrating the lava crust.

Based on the simplified nature of the experiments, we suggest caution in quantitatively comparing our data with gas-pistons activity observed in volcanic systems, nevertheless, a few additional analogies could be drawn. A linear or decreasing trend of the fluid surface during its ascent was noticed in our samples (Figure 6c), which is in accordance with the observations at lava lakes [*Orr and Rea*, 2012]. The extent of increase in the height of the surface ($\approx$0.002–0.01 m), scaled to the diameter of the experimental conduit (0.02 m) lies in the range of 0.1–0.5. A similar spectrum of normalized growth height (0.14–1.06) can be obtained from literature for gas-piston activity [*Orr and Rea*, 2012] (vent diameter: 5 m, piston height 0.7–5.3 m), suggesting that the extent of foam oscillation is rather similar.

The lifetime of a gas-piston ranges from few minutes to hours at the same vent [e.g., *Swanson et al*., 1979; *Orr and Rea*, 2012]. Similarly, in our experiments, we observed a range of growth and collapse time scales from few seconds to minutes. Such wide range of bursting probabilities fits properly with the broad distribution expected in foams [*Neethling et al*., 2005]. Nonetheless, in our experiments the ratio between average rising time and average collapse time is equal to $\approx$4.5 (average rise time: 77.5 s; average collapse time: 15 s), where the same ratio is much higher and equal to $\approx$ 16 in *Orr and Rea* [2012] (average rise time: 13 min, average collapse time: 49 s). In other words, our analogue foam experienced either longer collapse or shorter growth phases.

We recall here that our experiments do not take into account the effect of thermal heat exchange that are operative in lava lakes. On a long-term scale, the ascent of hot buoyant magma, replacing the cool and the crystallized outermost section, prevents the cooling and the death of the lava pool. This process has granted the long-term life of lava lakes such Erta-Ale, Ethiopia ($>$98 years) [*Harris et al*., 2005]. On the contrary, the lifetime of our experiments is dictated by the complete degassing of the sample. In addition, the heat exchange, occurring at the surface of the lava lake, generates a cool thin fractured crust lying above a ductile and viscoelastic layer with temperature comprised between 800 and 1070°C [*Harris*, 2008]. Beneath the viscoelastic layer, bubbles gather into a shallow foam with thickness of up to few tens of meters [*Chouet and Dawson*, 2015]. The crustal lid [*Swanson et al*., 1979] and/or the viscoelastic layer [*Patrick et al*., 2011] have been suggested to retain the gas phase during gas-piston growth. On the contrary, models based on the spontaneous foam collapse at the top of the lava lake assume that the crust is rather the consequence of foam accumulation, acting as rheological barrier [e.g., *Dibble*, 1972; *Orr and Rea*, 2012; *Chouet and Dawson*, 2015]. Whether it represent the mechanism for gas trapping or not, the superficial crust acts as an overburden that might contribute to stabilize the foam [*Chouet and Dawson*, 2015]. Hence, the occurrence of shorter growth phases agrees with the simplified nature of the experiments, where the contribution of the crust/viscoelastic layer is not present. An impermeable layer could further contribute retaining the foam during the drainage phase, increasing the time scale required for the onset of permeability and outgassing. In contrast, the extent of foam collapse depends on the liquid profile content, which is function of the bubble size distribution, the surface tension [*Neethling et al*., 2005] and of the properties of the foam. Nevertheless, we note that repeated foam collapse outgassing at the top of the fluid column of the analogue basaltic samples produces oscillations of the foam surface with similar features (e.g., scaled oscillation amplitude, linear or decelerating trend of the surface uplift) to those observed at lava lakes during gas-piston activity

(e.g., in Kilauea), and support the validity of gas accumulation models in explaining cyclic degassing style at basaltic volcanoes.

6. Concluding Remarks

1. Upon decompression of volatile-saturated samples, we observe the development and growth of a foam layer at the top of the analogue magma column. The foam enters into a regime of vigorous oscillation related to the repeated collapse of the outermost section.
2. Time scales of foam growth and collapse span over the range of $10–10^2$ s, with minimum values related to low fluid viscosities and high solid loading. The obtained results are up to 1 order of magnitude smaller than the time scale estimated from drainage. This misfit is attributed to the dominant contribution of the film thinning (hence coalescence and outgassing) of strain due to vertical ascent and bubble (decompressive or diffusive) growth. Additionally, the oscillation time scales are distributed in a relatively broad range, consistent with the complexity of the foam nature and the multiplicity of factors contributing to its coalescence.
3. Particle-bearing experiments in the semidiluted regime showed a shorter time scale of foam growth and collapse, which was related mainly to the role of solid network, increasing bubble breakup and coalescence. Additionally, the oscillation time scale increases with elapsed time, due to the hindering role of particles in redistributing the liquid involved in the precedent bursting phases.
4. Based on the similarity between our results (on fluid surface displacement trend and its amplitude) and observation of volcanic gas-piston activity, we showed that our simplified experimental system provides a good source model for gas-piston activity, confirming experimentally the validity of those models based on foam accumulation within the shallow conduit.

Acknowledgments
The data used in this work were collected during experiments performed by the authors and they may be available upon request to the corresponding author. We wish to acknowledge A. Costa for the fruitful discussions and two anonymous reviewers for the improving comments. L.S. and B.S. wish to acknowledge the support of the EU Projects MED-SUV (grant 308665) and NEMOH (FP7-MC-ITN, grant 289976). C.C. acknowledges support from the AXA Research Fund. A.A.C. thanks Alexander von Humboldt Foundation for supporting her academic visits in LMU and Mexican Projects (CONACYT-101515; UNAM-PAPIIT IN106111; IN105716) for partial funding. D.B.D. acknowledges support of the ERC Advanced Grant (EVOKES, 247076).

References

Bani, P., A. J. L. Harris, H. Shinohara, and H. Donnadieu (2013), Magma dynamics feeding Yasur's explosive activity observed using thermal infrared remote sensing, *Geophys. Res. Lett.*, *40*, 3830–3835, doi:10.1002/grl.50722.

Belien, I. B., K. V. Cashman, and A. V. Rempel (2010), Gas accumulation in particle-rich suspensions and implications for bubble populations in crystal-rich magma, *Earth Planet. Sci. Lett.*, *297*(1–2), 133–140, doi:10.1016/j.epsl.2010.06.014.

Bhakta, A., and E. Ruckenstein (1997), Decay of standing foams: Drainage, coalescence and collapse, *Adv. Colloid Interface Sci.*, *70*, 1–124, doi:10.1016/S0001-8686(97)00031-6.

Buckingham, E. (1914), On physically similar systems: Illustrations of the use of dimensional equations, *Phys. Rev.*, *4*, 345–376.

Carey, R. J., M. Manga, W. Degruyter, D. Swanson, B. Houghton, T. Orr, and M. Patrick (2012), Externally triggered renewed bubble nucleation in basaltic magma: The 12 October 2008 eruption at Halema'uma'u Overlook vent, Kīlauea, Hawai'i, USA, *J. Geophys. Res.*, *117*, B11202, doi:10.1029/2012JB009496.

Carniel, R., E. Del Pin, R. Budai, and P. Pascolo (2005), Identifying timescales and possible precursors of the awake to asleep transition in EOG time series, *Chaos Solitons Fractals*, *23*(4), 1259–1266.

Chadwick, W. W., Jr., I. C. Wright, U. Schwarz-Schampera, O. Hyvernaud, D. Reymond, and C. E. J. de Ronde (2008), Cyclic eruptions and sector collapses at Monowai submarine volcano, Kermadec arc: 1998–2007, *Geochem. Geophys. Geosyst.*, *9*, Q10014, doi:10.1029/2008GC002113.

Chouet, B. A., and P. Dawson (2015), Seismic source dynamics of gas-piston activity at Kīlauea Volcano, Hawai'i, *J. Geophys. Res. Solid Earth*, *120*, 2525–2560, doi:10.1002/2014JB011789.

Cruz, F. G., and B. A. Chouet (1997), Long-period events, the most characteristic seismicity accompanying the emplacement and extrusion of a lava dome in Galeras Volcano, Colombia, in 1991, *J. Volcanol. Geotherm. Res.*, *77*(1), 121–158.

Dibble, R. R. (1972), Seismic and related phenomena at active volcanoes in New Zealand, Hawaii, and Italy, PhD dissertation, Victoria Univ., Wellington.

Druitt, T. H., S. R. Young, B. Baptie, C. Bonadonna, E. S. Calder, A. B. Clarke, P. D. Cole, C. L. Harford, R. A. Herd, R. Luckett, G. Ryan, and B. Voight (2002), Episodes of cyclic Vulcanian explosive activity with fountain collapse at Soufrière Hills Volcano, Montserrat, *Mem. Geol. Soc. London*, *21*, 281–306.

Edmonds, M., and T. M. Gerlach (2007), Vapor segregation and loss in basaltic melts, *Geology*, *35*, 751–754.

Fiege, A., F. Holtz, and B. C. Sarah (2014), Bubble formation during decompression of andesitic melts, *Am. Mineral.*, *99*, 1052–1062, doi:10.2138/am.2014.4719.

Gardner, J. E. (2007), Bubble coalescence in rhyolitic melts during decompression from high pressure, *J. Volcanol. Geotherm. Res.*, *166* (3-4), 161–176, doi:10.1016/j.jvolgeores.2007.07.006.

Giordano, D., C. Romano, P. Papale, and D. B. Dingwell (2004), The viscosity of trachytes, and comparison with basalts, phonolites, and rhyolites, *Chem. Geol.*, *213*(1-3), 49–61, doi:10.1016/j.chemgeo.2004.08.032.

Gonnermann, H. M., and M. Manga (2003), Explosive volcanism may not be an inevitable consequence of magma fragmentation, *Nature*, *426*, 432–435, doi:10.1038/nature02138.

Grassia, P., S. J. Neethling, C. Cervantes, and H. T. Lee (2006), The growth, drainage and bursting of foams, *Colloids Surf. A*, *274*(1), 110–124.

Harris, A. J. (2008), Modeling lava lake heat loss, rheology, and convection, *Geophys. Res. Lett.*, *35*, L07303, doi:10.1029/2008GL033190.

Harris, A. J., R. Carniel, and J. Jones (2005), Identification of variable convective regimes at Erta Ale lava lake, *J. Volcanol. Geotherm. Res.*, *142*(3), 207–223.

Iglesias, E., J. Anderez, A. Forgiarini, and J. L. Salager (1995), A new method to estimate the stability of short-life foams, *Colloids Surf. A*, *98*(1), 167–174.

James, M. R., J. L. Steve, and B. Houghton (2013), Unsteady explosive activity: Strombolian eruptions, in *Modeling Volcanic Processes: The Physics and Mathematics of Volcanism*, edited by S. A. Fagents, T. K. P. Gregg, and R. M. C. Lopes, pp. 107–128, Cambridge Univ. Press, N. Y.
Jaupart, C., and S., Vergniolle (1988), Laboratory models of Hawaiian and Strombolian eruptions, *Nature*, *331*, 58–60.
Jaupart, C., and S. Vergniolle (1989), The generation and collapse of a foam layer at the roof of a basaltic magma chamber, *J. Fluid Mech.*, *203*, 347–380.
Johnson J. B., A. J. L. Harris, and R. P. Hoblitt (2005), Thermal observations of gas pistoning at Kilauea volcano, *J. Geophys. Res.*, *110*, B11201, doi:10.1029/2005JB003944.
Llewellin, E. W., and M. Manga (2005), Bubble suspension rheology and implications for conduit flow, *J. Volcanol. Geotherm. Res.*, *143*, (1-3), 205–217.
Lomb, N. R. (1976), Least-squares frequency analysis of unequally spaced data, *Astrophys. Space Sci.*, *39*(2), 447–462.
Mader, H. M., E. W. Llewellin, and S. P. Mueller (2013), The rheology of two-phase mag-mas: A review and analysis, *J. Volcanol. Geotherm. Res.*, *257*, 135–158, doi:10.1016/j.jvolgeores.2013.02.014.
Mangan, M. T., K. V. Cashman, and D. A. Swanson (2015), The dynamics of Hawaiian-style eruptions: A century of study, in *Characteristics of Hawaiian Volcanoes, 2014*, edited by M. P. Poland, T. J. Takahashi, and C. M Landowski, chap. 8, pp. 323–354, U.S. Geological Survey.
Marchetti, E., and A. J. L. Harris (2008), Trends in activity at Pu'u 'O'o during 2001–2003: Insights from the continuous thermal record, in *Fluid Motions in Volcanic Conduits: A Source of Seismic and Acoustic Signals*, edited by S. J. Lane and J. S. Gilbert, *Geol. Soc. Spec. Publ.*, *307*, 85–101.
Mena, P. C., M. C. Ruzicka, F. A. Rocha, J. A. Teixeira, and J. Drahoš (2005), Effect of solids on homogeneous–heterogeneous flow regime transition in bubble columns, *Chem. Eng. Sci.*, *60*, 6013–6026.
Mueller, S., E. W. Llewellin, and H. M. Mader (2010), The rheology of suspensions of solid particles, *Proc. R. Soc. A*, *466*, 1201–1228, doi: 10.1098/rspa.2009.0445.
Namiki, A., and M. Manga (2006), Influence of decompression rate on the expansion velocity and expansion style of bubbly fluids, *J. Geophys. Res.*, *111*, B11208, doi:10.1029/2005JB004132.
Neethling, S. J., H. T. Lee, and P. Grassia (2005), The growth, drainage and breakdown of foams, *Colloids Surf. A*, *263*(1-3), 184–196, doi: 10.1016/j.colsurfa.2004.12.014.[10.1016/j.colsurfa.2004.12.014]
Nguyen, C. T., H. M. Gonnermann, Y. Chen, C. Huber, A. A. Maiorano, A. Gouldstone, and J. Dufek (2013), Film drainage and the lifetime of bubbles, *Geochem. Geophys. Geosyst.*, *14*, 3616–3631, doi:10.1002/ggge.20198.
Okumura, S., M. Nakamura, A. Tsuchiyama, T. Nakano, and K. Uesugi (2008), Evolution of bubble microstructure in sheared rhyolite: Formation of a channel-like bubble network, *J. Geophys. Res.*, *113*, B07208, doi:10.1029/2007JB005362.
Oppenheimer, J., A. C. Rust, K. V. Cashman, and B. Sandnes (2015), Gas migration regimes and outgassing in particle-rich suspensions, *Frontiers Phys.*, *3*, 60, 1–13, doi:10.3389/fphy.
Orr, T. R., and J. C. Rea (2012), Time-lapse camera observations of gas piston activity at Pu'u 'Ō 'ō, Kīlauea volcano, Hawai'i, *Bull. Volcanol.*, *74*(10), 2353–2362.
Patrick, M. R., T. Orr, D. Wilson, D. Dow, and R. Freeman (2011), Cyclic spattering, seismic tremor, and surface fluctuation within a perched lava channel, Kīlauea Volcano, *Bull. Volcanol.*, *73*(6), 639–653.
Patrick, M. R., T. Orr, L. Antolik, L. Lee, and K. Kamibayashi (2014), Continuous monitoring of Hawaiian volcanoes with thermal cameras, *J. Appl. Volcanol.*, *3*(1), 1–19, doi:10.1186/2191−5040-3-1.
Patrick, M. R., T. Orr, A. J. Sutton, E. Lev, W. Thelen, and D. Fee (2016), Shallowly driven fluctuations in lava lake outgassing (gas pistoning), Kīlauea Volcano, *Earth Planet. Sci. Lett.*, *433*, 326–338.
Proussevitch, A. A., D. L. Sahagian, and V. A. Kutolin (1993), Stability of foams in silicate melts, *J. Volcanol. Geotherm. Res.*, *59*(1), 161–178.
Rathbun, J. A., J. R. Spencer, A. G. Davies, R. R. Howell, and L. Wilson (2002), Loki, Io: A periodic volcano, *Geophys. Res. Lett.*, *29*(10), doi: 10.1029/2002GL014747.
Rust, A. C., M. Manga, and K. V. Cashman (2003), Determining flow type, shear rate and shear stress in magmas from bubble shapes and orientations, *J. Volcanol. Geotherm. Res.*, *122*, 111–132, doi:10.1016/S0377-0273(02)00487-0.
Scargle, J. D. (1982), Studies in astronomical time series analysis. II-Statistical aspects of spectral analysis of unevenly spaced data, *Astrophys. J.*, *263*, 835–853.
Sparks, R. S. J. (1978), The dynamics of bubble formation and growth in magmas: A review and analysis, *J. Volcanol. Geotherm. Res.*, *3*, 1–37.
Spina, L., et al. (2016a), Explosive volcanic activity at Mt. Yasur: A characterization of the acoustic events (9–12th July 2011), *J. Volcanol. Geotherm. Res.*, doi:10.1016/j.jvolgeores.2015.07.027, in press. [Available at http://www.sciencedirect.com/science/article/pii/S0377027315002358.]
Spina, L., C. Cimarelli, B. Scheu, D. Di Genova, and D. B. Dingwell (2016b), On the slow decompressive response of volatile-and crystal-bearing magmas: An analogue experimental investigation, *Earth Planet. Sci. Lett.*, *433*, 44–53.
Swanson, D. A., W. A. Duffield, D. B. Jackson, and D. W. Peterson (1979), Chronological narrative of the 1969–71 Mauna Ulu Eruption of Kilauea Volcano, Hawaii, *U.S. Geol. Surv. Prof. Pap.*, *1056*, 55 pp.
Tilling, R. I. (1987), Fluctuations in surface height of active lava lakes during 1972–1974 Mauna Ulu Eruption, Kilauea Volcano, Hawaii, *J. Geophys. Res.*, *92*(B13), 13,721–13,730, doi:10.1029/JB092iB13p13721.
Wilson, L., and J. W. Head (1981), Ascent and eruption of basaltic magma on the Earth and Moon, *J. Geophys. Res.*, *86*, 2971–3001.
Wilson, L., R. S. J. Sparks, and G. P. L. Walker (1980), Explosive volcanic eruptions-IV. The control of magma properties and conduit geometry on eruption column behaviour, *Geophys. J. R. Astron. Soc.*, *63*, 117–148.
Witham F., A. W. Woods, and C. Gladstone (2006), An analogue experimental model of depth fluctuations in lava lakes, *Bull. Volcanol.*, *69*(1), 51–56.